THE ASTROPHYSICAL JOURNAL, 370:355–369, 1991 March 20

A CRITICAL ANALYSIS OF THE ULTRAVIOLET TEMPERATURE SCALE OF THE HELIUM-DOMINATED DB AND DBV WHITE DWARFS

PETER THEJLL, STÉPHANE VENNES, AND HARRY L. SHIPMAN
Department of Physics and Astronomy, Sharp Laboratory University of Delaware, Newark, DE 19716
Received: 1990 June 18; accepted 1990 September 4

ABSTRACT

The temperatures of the hottest of the DB and of some of the variable DBV white dwarfs have been reanalyzed, using a new helium-rich model atmosphere grid and archival *IUE* data. The grid covers variations in the effective temperature, surface gravity, and trace hydrogen abundance. We find significantly lower temperatures than those found by earlier investigations. This has influence on the issue of which mixing-length theory is the best one for treatment of convection in DB white dwarfs. The prototype of the DBV stars, GD 358, is given particular attention in view of the recently reported He II λ1640 line. We analyze the sensitivity of the new results to input physics. We find that uncertainties in Stark broadening parameters, convective efficiency, and equation of state and the assumptions of a fixed gravity ($\log g = 8$) and a negligible abundance of hydrogen can at most give an error in the effective temperature of 400 K for a typical DB star. The uncertainty on the absolute calibration of the *IUE* cameras and the effect of small interstellar reddening dominate the error analysis.

Subject headings: stars: atmospheres — stars: individual (GD 358) — stars: white dwarfs — ultraviolet: spectra

1. INTRODUCTION

The helium-rich DB white dwarfs have been studied for quite some time, and intensely so since the discovery of the variability of some of them, the DBV stars. In 1982, Winget et al. reported that the DB star GD 358 (WD 1645+323) showed brightness variations of 0.3^m with a period of 600 to 700 s. Theoretical studies by Winget et al. (1983) and Fontaine, Tassoul, & Wesemael (1984) described the mechanism for the pulsations and the properties of the DBV stars. At the bottom of the convective surface layer the partial ionization zone is unstable to perturbations, as in the hydrogen-rich ZZ Ceti stars, and may drive the pulsation if the thermal time scale of the zone is of the order of the pulsation periods. Conditions in the zone are sensitive to the efficiency of convection; in this link between pulsations and convection lies the possibility of using observations of DBV stars to better understand convection. In particular Fontaine et al. (1984) saw a way to calibrate the mixing-length ratio, which is a free parameter used in simple convection theories.

Because convective energy transport is so effective, even small changes in the modeling of the mechanism can alter strongly the structure of a convective layer. A full discussion of the details of convective energy transport is beyond the scope of this paper and the interested reader may wish to read de Loore (1970), Böhm & Cassinelli (1971), Böhm & Grenfell (1973), or Fontaine, Villeneuve, & Wilson (1981). The last paper contains a description of the mixing-length theories, referred to as ML1, ML2 or ML3.

GD 358 is the brightest and best studied DBV star, but the determination of its atmospheric parameters is still the subject of current research (Winget et al. 1982; Koester, Weidemann, & Vauclair 1983; Koester et al. 1985, Liebert et al. 1986; Sion et al. 1988). Early discoveries of the DBV stars underscored the difficulty of predicting the variability of a DB star, based on its optical spectrum. A general problem for the measurement of $T_{\rm eff}$ and $\log g$ for DB and DBV stars is that in their temperature range (up to $\sim$30,000 K) the sensitivity of optical He I lines to changes in these parameters is quite low. But, because the theory of pulsation gives detailed predictions of such DBV properties, much effort has been put into the analysis of these stars. Pulsations are predicted to exist in a narrow temperature range, only 3000 K wide (Winget et al. 1983). It is hard to determine $T_{\rm eff}$ with an accuracy of even half this amount using optical data alone. In 1986, Liebert et al. (hereafter L86) presented a comprehensive analysis of all the then-known DBV (Winget et al. 1984; Winget, Nather, & Hill 1987) and some DB stars using *IUE* data and several model atmosphere grids (Koester 1980; Wesemael 1981, hereafter W81; Wickramasinghe 1983). Since then more DBV stars have been found, all apparently falling consistently in the same temperature range (Grauer et al. 1988, 1989). The temperature range found for the DBV stars in L86 supported the use of ML3 when predicting the pulsation properties of the convective helium dominated models.

Considerable interest is focused on the accurate determination of atmospheric parameters for DB white dwarfs, for yet another reason. The so called "DB gap" between 30,000 and 45,000 K, in which no helium-rich white dwarfs are observed, is an observational feature that any model seeking to explain evolution of white dwarfs should address (MacDonald & Vennes 1990). Since the limits of this forbidden region may have more to do with the timing of physical changes in the individual stars surrounding it, its placement is less amenable to quantitative analysis than are the properties of the DBV stars.

The *IUE* data we use in this paper were acquired with NASA's Regional Data Analysis Facility at Goddard Space Flight Center. Some *IUE* and optical data for DB and DBV white dwarfs have been published by Oke (1974), Wickramasinghe & Whelan (1977), Koester et al. (1983), Wick-

ramasinghe (1983), Wickramasinghe & Reid (1983), Greenstein (1984), Oke, Weidemann, & Koester (1984), Koester et al. (1985), L86, Wegner & Nelan (1987), Reid et al. (1988), and Greenstein & Liebert (1990).

In this paper we focus on re-analyzing the *IUE* data for the stars analyzed in L86 for two reasons: the knowledge of the sensitivity degradation with time of the *IUE* cameras has considerably improved since L86, and our analysis is performed in the light of a new comprehensive grid of helium-blanketed model atmospheres.

In § 2 we discuss the influence of input physics on the model atmospheres and synthetic spectra that are used to fit observations. In § 3 we compare our models to other published and unpublished models. In § 4 we apply our models to the existing *IUE* data and derive new effective temperatures for some DB and DBV white dwarfs. In §§ 5 and 6 we discuss the results and draw conclusions. Finally, we include in a table an excerpt from our new model grid for DB white dwarfs (pure helium, 19,000 K $\leq T_{\rm eff} \leq$ 30,000 K, log g = 8, ML2).

2. THE IMPORTANCE OF THE INPUT PHYSICS

We have analyzed the influence of convective theories, treatment of the equation of state, and the use of different opacities on the helium-dominated models calculated using a version of the model atmosphere program ATLAS (see Kurucz 1970). We also studied the effects of variations in temperature and trace amounts of hydrogen. Our basic grid includes models at 19,000, 20,800, 21,600, 22,500 25,000, 27,500, and 30,000 K, for log g = 7.5, 8.0, and 8.5. Figure 1 is the calculated Eddington flux for the sequence of temperatures, log g = 8, and ML2. Figure 2 is the calculated Eddington flux for $T_{\rm eff}$ = 25,000 K, ML2 at several gravities. For an application to the DBA white dwarfs (Bhatia et al. 1989), the grid covers the hydrogen abundances log [n(H)/n(tot)] = −9, −8, −7, −6, −5, and −4 at log g = 8 and the selected temperatures [throughout this paper any element concentration refers to the relative abundance by number: n(element)/n(tot)]. All models include the blanketing effect of optical and ultraviolet He I and He II lines

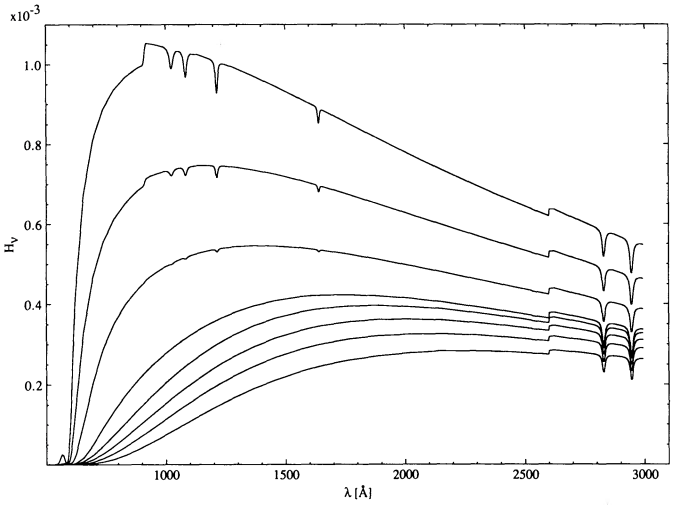

FIG. 1.—Ultraviolet Eddington flux (ergs cm^{-2} s^{-1} Hz^{-1} steradian^{-1}) from the sequence of pure He models at log g = 8. The synthetic spectra have been convolved with a 7 Å wide Gaussian. The effective temperatures of the models are, from the bottom, 19,000, 20,000 20,800, 21,600, 22,500, 25,000, 27,500, and 30,000 K. The He I lines in the 2800–3000 Å range can be seen in some low-resolution *IUE* exposures.

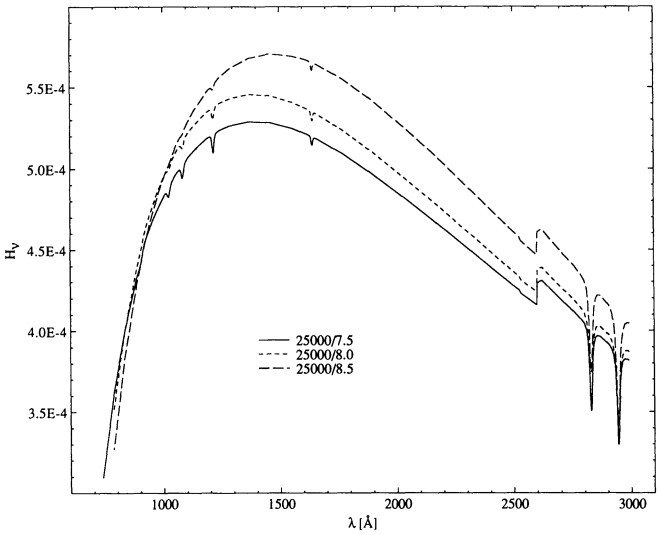

FIG. 2.—Same as Fig. 1, but for the models at $T_{\rm eff}$ = 25,000 K and log g = 7.5, 8.0, amd 8.5.

(and H I lines when applicable). We have tested the ML1, ML2 and ML3 convection theories on the log g = 8 models, and the influence of different equations of state on a few critical ones. The results of these calculations are summarized in § 2.7.

2.1. *Influence of Hydrogen*

We first investigate the influence of trace amounts of hydrogen on the determination of the ultraviolet temperatures of the DB and DBV white dwarfs. Bhatia et al. (1989) suggest that there may be low levels of hydrogen, typically less than 10^{-6}, in the hot DB white dwarfs. What is the quantitative influence of such trace amounts of hydrogen on the temperature determination, if continuum flux levels are used for fitting models to ultraviolet fluxes?

The relationship between effective temperature and continuum flux level is well represented by

$$T_{\rm eff} = 48{,}228 - 54{,}679{*}{\rm H} + 30{,}618{*}{\rm H}^2 - 4780{*}{\rm H}^3 , \quad (1)$$

where the V-normalized Eddington flux at λ = 1850 Å is

$$\mathrm{H} = \frac{\mathrm{H}_\nu(1850\ \text{Å})}{\mathrm{H}_\nu(5500\ \text{Å})} ,$$

and $T_{\rm eff}$ is the effective temperature in Kelvin. This expression is valid between 19,000 and 30,000 K at log g = 8.0 for our pure helium models. The maximum sensitivity of $T_{\rm eff}$ to the ultraviolet flux in the range of the *IUE* cameras (SWP 1150–1950 Å, LWR(P) 1950–3200 Å) is found between 22,000 and 27,000 K, where a 1% change in the flux level corresponds to at least a 100 K change in $T_{\rm eff}$.

The continuum flux level of our models, at 1850 Å, rises no more than 0.8% above the flux levels of pure helium models when the hydrogen concentration n(H)/n(tot) is increased from 10^{-5} to 10^{-4} at 22,500 K, and increases only about half as much (0.3%) at 27,500 K. The change when altering n(H)/n(He) from 0 up to 10^{-5}, in both cases, is essentially zero. Thus the effect, on the derived effective temperature, of neglecting the actual abundance of hydrogen within a DB star is less than 100 K.

How well can one independently limit the hydrogen abundance in a DB star or determine it in a DBA white dwarf using

TABLE 1

EQUIVALENT WIDTH OF THE H λ1215.67 + He II λ1215.13 COMPLEX

log [n(H)/n(He)]	W (22,500 K)[a] (Å)	W (27,500 K) (Å)
Pure helium	0.009	0.455
−9	0.010	0.455
−8	0.022	0.452
−7	0.119	0.471
−6	0.402[b]	0.584
−5	1.104	0.877[b]
−4	2.829[c]	1.634
−3	...	...[c]

[a] W is the equivalent width at the specified effective temperature (22,500 or 27,500 K).

[b] At this abundance of hydrogen the contribution of H Lyα is detectable.

[c] At this abundance, the hydrogen content starts to influence the continuum flux.

IUE observations of Lyα? The hydrogen contribution to the equivalent width of the λ1215 line becomes detectable (at the ≈0.5 Å level) when the hydrogen concentration rises past $10^{-6.5}$ at 22,500 K since there is virtually no contribution to the λ1215 line from He II. At 27,500 K the line has $a \approx 0.5$ Å width contribution from He II $n = 2$–4. Assuming that other data have fixed $T_{\rm eff}$ at 27,500 K, then any hydrogen admixture becomes noticeable at the $w \approx 0.5$ Å level (*above* the He II contribution) at a hydrogen concentration of $10^{-5.5}$ or more. Since hydrogen is detectable in the λ1215 line before there is any important influence on the flux level, the absence of the hydrogen-contribution at the ≈0.5 Å level will ensure that no errors above the 1% level in the continuum flux are introduced. This procedure does require that the geocoronal emission is not so strong that it hinders measurement of the λ1215 lines equivalent width or fitting of the red wing of this line in the *IUE* data. The equivalent width of the Lyα + He II λ1215 line as a function of hydrogen concentration at two temperatures typical for DB stars is shown in Table 1.

2.2. *Gravity*

In Table 2, we present the results of a sensitivity analysis wherein we see what effect an uncertainty in log g of ±0.3 (Shipman 1979) can have on the subsequent determination of $T_{\rm eff}$. We have found that by picking a model of a DB star that has the wrong gravity by as much as ±0.3 in log g the effective temperature, derived by fitting the V-normalized UV flux to *IUE* observations (represented by a typical wavelength of 1850 Å), can be expected to have an error of 300 K at 22,500 K and only 50 K at 19,000 K and 30,000 K. The temperature analysis of the DB and DBV stars is therefore not very sensitive to the assumed gravity.

TABLE 2

SENSITIVITY OF $T_{\rm eff}$ TO THE UNCERTAINTY IN LOG g

$T_{\rm eff}$ (K)	ΔH[a]	$\Delta T_{\rm eff}$[b] (K)
30,000	0.6	30
25,000	1.8	180
22,500	3.0	300
19,000	0.9	45

[a] ΔH is the relative change in H, in percent for an uncertainty in log g of 0.3. H is the model flux at 1850 Å divided by the flux at 5500 Å.

[b] $\Delta T_{\rm eff}$ is the uncertainty in $T_{\rm eff}$.

2.3. *Convection Theories: ML1/ML3*

Various convective theories of the mixing-length formalism are described as ML1, ML2 and ML3, depending on the choice of certain physically meaningful parameters (Fontaine et al. 1981). ML1 is the formalism that results in the least efficient convective energy transport of the three. ML3 is similar to the ML2 formalism with the mixing-length ratio increased from 1 to a value of 2. The efficiency at which energy is transported through a stellar photosphere influences the temperature distribution and this in turn determines the particle densities and opacities so that the calculated emergent flux becomes sensitive to the convection theory used. In DB stars at temperatures below 25,000 K or so, the convection zone in the deeper parts of the envelope has moved so close to the surface that it emerges into the photosphere (Rosseland optical depth about unity) and starts to have influence on the calculated emergent flux.

We compared the flux from ML3 models to that in ML1 models. The more efficient ML3 convection theory tends to lower the temperature at the base of the photosphere ($\tau_{\rm R} \approx 100$) and raises it in the line-formation region ($\tau_{\rm R} \approx 1$). For the typical temperatures we have investigated we found that the temperature fall at depth did not influence either the continuum or line fluxes. The slight warming that took place at about Rosseland optical depth unity did cause continuum fluxes to change, raising the V-normalized ultraviolet flux by 1.4% for models from 19,000 K up to about 22,000 K. It then drops to less than 0.5% at 22,500 K and falls to the 0.07% level at 30,000 K. The maximum error introduced by using an inappropriate mixing length theory on $T_{\rm eff}$ is thus no more than 170 K up to about 23,000 K and less than 50 K at higher temperatures. This is in sharp contrast with the ZZ ceti stars (the DAV) for which the fitted effective temperatures depend strongly (up to 500 K) on the parameters chosen to describe the convection zone (Fontaine et al. 1984).

2.4. *Equation of State*

The treatment of the model atom has some importance on the calculated emerging flux. In the DB photosphere most of the helium is in the neutral state and the upper levels of the atom may be significantly populated. A truncation of the summation over states, when calculating partition functions, affects the electron density and the resulting ionization balance which in turn influences the calculated emergent flux. A simple prescription is to use a constant number of levels through the atmosphere as in W81. A second possibility (used in this work) is to truncate the helium and hydrogen partition functions using the Debye-Hückel formalism. Höhne & Zimmermann (1982) discuss some aspects of the Debye-Hückel theory.

The influence on the continuum flux was no more than 0.3% when comparing two separately converged models at 22,500 K/log $g = 8$ using the two different treatments: a fixed number of levels and the Debye-Hückel cutoff. Between converged models the difference in the predicted ultraviolet temperature is thus much less than 100 K. This is due to the fact that the Rosseland depth scale adjusted itself, relative to the mass-loading scale, to a change in electron density in such a way that the fundamental relations $T(\tau_{\rm R})$ and $n_e(\tau_{\rm R})$ remain nearly unal-

terated. The solution of the radiative transfer equation is obtained relative to the Rosseland scale. To recover the synthetic spectrum consistent with a specific structure, one has to use the same modeling of the atomic partition functions or to impose the electron density given by the original model. We imposed this last condition when calculating a synthetic spectrum from the published model atmospheres of W81.

2.5. *Solving the Radiative Transfer Equation*

During calculation of a model atmosphere, the iterative process is performed until some pre-chosen tolerance is achieved. In ATLAS, convergence is typically halted when the total flux (convective + radiative) is equal to

$$H_{tot} = \frac{\sigma T_{eff}^4}{4\pi} \quad (2)$$

to within 1% or 0.1% at all depth levels. The influence of this on the effective temperature of a typical DB/DBV star is less than 50 K.

We found that the influence of the choice of depth grid and frequency sampling is unimportant to the general structure of the converged model. For instance, we used the W81 depth grid and 180 point frequency grid to converge a model at $T_{eff} = 25{,}000$ K, and then did the same with a 1500 point frequency grid. The emergent flux from the two models were consistent within 1% of error.

2.6. *Opacity Considerations in ATLAS*

We have exchanged the bound-free cross sections for He I originally in ATLAS (see Kurucz 1970) for the improved cross sections of Koester et al. (1985). Except for the $1\,^1S$ and $2\,^2S$ bound-free transitions, the old ATLAS cross sections are the same as those of W81. The actual changes in the emergent flux, due to these new cross-sections, are very minor, much less than 1%.

The lines that cause most of the blanketing are the strong He I resonance lines and to a lesser extent the group of strong neutral helium lines in the visible range of the spectrum, notably He I λ4471. Most of our He I lines are modeled by Voigt profiles, broadened by electron and ion interactions, using data from Dimitrijevic & Sahal-Brechot (1984a, b) and occasionally from Griem (1974), the latter only for broadening due to electrons. For some lines there is a detailed treatment: for He I λ4471, which is the strongest optical line, we used the theory of Barnard, Cooper, & Shamey (1969). This is also the case for He I λ4922. The series limits are not modeled in detail and only a limited number of lines are included. The use of more lines merged together near the series limit according to the Inglis-Teller prescription would give smoother photoionization edges.

We have not used the Griem (1974) theory as employed by W81 to model most He II lines but use instead the Auer & Mihalas (1972) formalism. However, no He II line is strong enough at typical DB temperatures to affect the blanketing. We modeled He II λ1215 by the Auer & Mihalas (1972) formalism, but we use the Schöning & Butler (1989a, b) profile for He II λ1640. The Schöning & Butler (1989a, b) profiles include a convolution with the Doppler core making them very accurate for detailed modeling of small features.

We tested the influence of using He I Stark widths that were larger by factors of 2 to 5 and found that the effect on the model at 25,000 K/log $g = 8$ was small. The effect on the V-magnitude normalized flux was less than 3% in the ultraviolet spectral range while the effect on the flux normalized at 1850 Å was practically nonexistent above 1000 Å. On the red wing of the strong He I line at 584 Å the effect was noticeable. Since most Stark widths are accurate to 20% or 30% the effect of this error on the emergent ultraviolet flux will be less than 1%.

Thus, the influence of different blanketing due to different line-broadening treatments in the various model atmosphere codes we are discussing, and the small effect of different bound-free opacities, cannot give changes in the continuum flux larger than 1% or 2%. The influence of the uncertainty in opacity is thus smaller than 200 K on T_{eff}.

2.7. *Conclusions of Our Sensitivity Analysis*

The largest total error that could be introduced by making, at the same time, the worst choice of H abundance, gravity, mixing-length theory and equation of state, as well as the other sources of errors discussed above, is given by the sum of squares of the errors cited above:

$$\begin{aligned}(\Delta T_{eff})^2 &\le (\Delta T_{[n(H)/n(He)]})^2 + (\Delta T_g)^2 + (\Delta T_{ML})^2 \\ &\quad + (\Delta T_{eq.\ state})^2 + (\Delta T_{convergence})^2 + (\Delta T_{bl})^2 \\ &= (100\text{ K})^2 + (300\text{ K})^2 + (150\text{ K})^2 \\ &\quad + (100\text{ K})^2 + (100\text{ K})^2 + (200\text{ K})^2 \\ &\approx (430\text{ K})^2 . \end{aligned} \quad (3)$$

Here each term corresponds to a typical error introduced into the effective temperature determination from one of the six considered sources of error.

So, over and above the errors due to uncertainties in the observational data, the temperature determination, using the type of models we describe here, we will have at most an error of 430 K, which is generally less than the errors introduced by uncertainties in the flux measurements, such as the ultraviolet flux and the V-magnitude. The *IUE* flux calibration is often said to be known to within $\pm 10\%$, and we assume that any V-magnitude is accurate to $\pm 0.05^m$ which corresponds to a flux error of roughly $\pm 5\%$. If we set the total uncertainty on the overall observed flux level to about $\pm 10\%$, this type of error on the effective temperature may amount to ± 1000 K at 22,500 K or ± 500 K at 19,000 K and 30,000 K.

3. COMPARING TO OTHER MODEL GRIDS

We compared our grid to models published or kindly provided for us by Detlev Koester and François Wesemael (1990). The model provided by D. Koester is helium line blanketed and is not the same as the Koester (1980) models used in L86 which included blanketing due to small traces of hydrogen only. The new model provided by F. Wesemael is helium line blanketed as in Wesemael (1981). The published models we compared to are those of Wesemael (1981) and those of Wegner & Nelan (1987).

Wegner & Nelan (1987) presented blanketed DB models with temperatures up to 23,000 K. We compared our model at 20,000 K/log $g = 8$ to their corresponding model and got an agreement between the V-magnitude normalized fluxes better than 4% in the range covered by the *IUE* SWP and LWR cameras (Fig. 3). A 4% difference corresponds roughly to 400 K in its effect on T_{eff} in agreement with the expected uncertainty derived in the sensitivity analysis above.

When we compared the 25,000/8 model flux from our grid

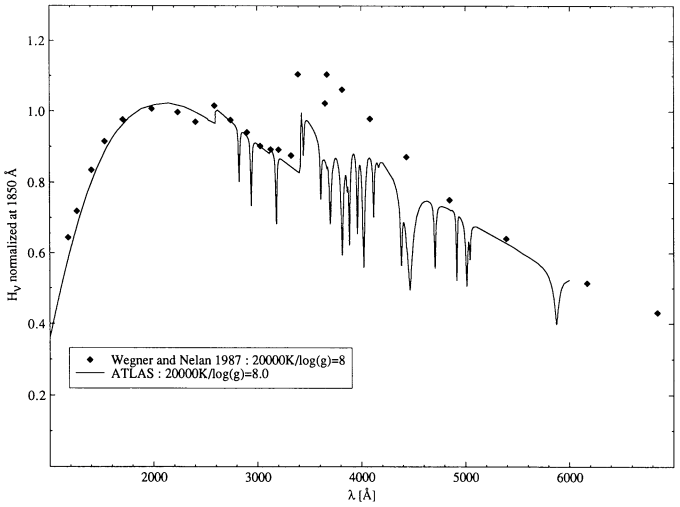

FIG. 3.—Blanketed model by Wegner & Nelan (1987) at 20,000 K, log $g = 8$ compared to one from ATLAS. The flux coincides in both models at 1850 and 5500 Å. The largest flux difference of 4% corresponds to roughly a 180 K effective temperature difference.

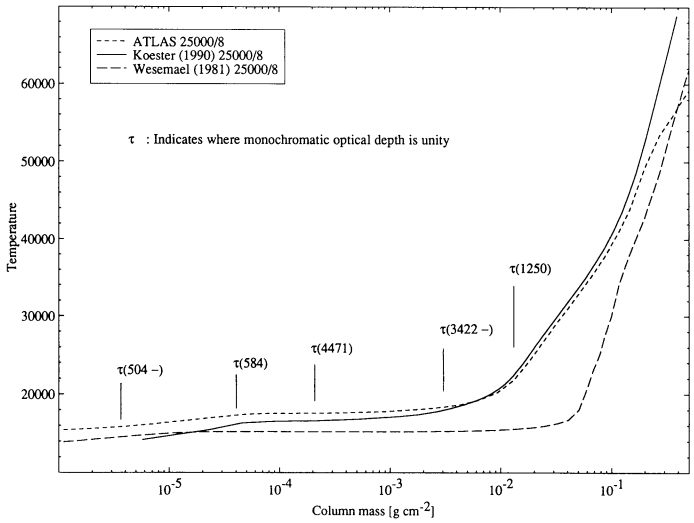

FIG. 5.—Comparison between the temperature stratification of models at 25,000 K and log $g = 8$. The dissimilarity between the Wesemael (1981) synthetic spectrum and the others (Fig. 4) is also evident in the temperature stratification. Optical depths unity at various wavelengths are indicated.

with that of the new Koester (1990) and Wesemael (1990) models, we found very good agreement. The difference between the fluxes in the 1200–1900 Å range amounted to at most 5%, corresponding to at most a 500 K temperature difference when using V-magnitude normalized fluxes (Fig. 4*b*). When using normalization at 1850 Å, as was done in L86, the similarity between Koester (1990) and Wesemael (1990) new models and the ATLAS model is nearly perfect in the relevant range; the difference is nowhere greater than 0.2% (Fig. 4*a*). The comparison to the blanketed W81 model was less satisfactory, however. That discrepancy is illustrated by a comparison of the temperature stratifications in Figure 5.

In summary, we have analyzed the influence, and the correctness, of the input physics of ATLAS and been able to show close correspondence between the models ATLAS produces and recent models of Koester (1990) and Wesemael (1990). We have not been able to reproduce the models of the W81 grid at 25,000 K (Figs. 4 and 5) and at 30,000 K. The input physics that a model depends on has been shown to not have the potential for causing the magnitude of differences we see between our model and that of W81. Since there is no difficulty with reproducing its unblanketed models, the cause of the differences between our models and the blanketed models of W81 may have something to do with the application of blanketing. We note that the W81 blanketed emergent flux of the 25,000 K/log $g = 8$ model is consistent with the W81 temperature stratification, but that the integral of the flux does not satisfy equation (2). The integrated flux of the blanketed model (published without lines) is about 20% lower than the value predicted by the effective temperature. Adding line profiles that we calculate, using the same physics as in W81, we get a discrepancy of 50%. In the next section we re-analyze the available DB and DBV *IUE* data with our new model grid.

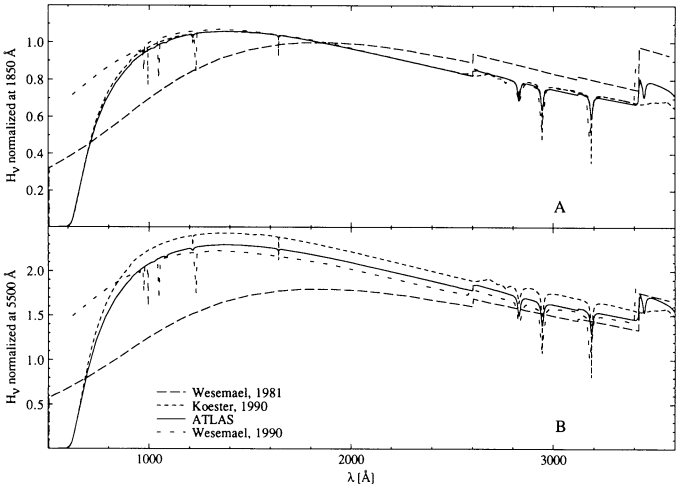

FIG. 4.—(*a*) Comparison between the emergent flux of models at 25,000 K and log $g = 8$; W81, Wesemael (1981); Koester (1990); ATLAS, present study; W90, Wesemael (1990). All synthetic spectra have been normalized at $\lambda = 1850$ Å. (*b*) Same as Fig. 4*a*, but with the synthetic spectra normalized at $\lambda = 5500$ Å.

4. ANALYSIS OF THE DB AND DBV STARS

The comparison of the theoretical spectra with the ultraviolet observations of the hot DB white dwarfs obtained with *IUE* takes two complementary approaches. We use first a method relying on the shape of the observed UV spectrum by choosing to normalize the synthetic spectrum to a wavelength in the UV range itself. That experiment may be repeated for two or three widely separated 100 Å wide bins, chosen for their smoothness: 1850 Å (the choice of procedure in L86), and another bin in the range 2500–2900 Å. To complete the analysis, the optical magnitude V Johnson (alternatively Strömgren y) or MCSP V is chosen as a normalizing pivot because of its relative isolation from the strong He I lines. A unique solution to the effective temperature should be obtained for these two normalization procedures.

The girds are defined principally in the ($T_{\rm eff}$, log g) space of parameters with some complementary parameters discussed previously [n(H)/n(He), ML theory]. In the course of the analysis, it became apparent that another parameter should be included, E_{B-V}, the interstellar extinction coefficient. We used the Seaton (1979) extinction law. We have used this parameter as a means to improve the statistical quality of the fit as well as

a means to reconcile the solutions obtained with our two complementary normalization procedures. We found that the effect of a small extinction coefficient is to depress considerably the ultraviolet flux relative to the optical flux without alterating the "shape" of the ultraviolet spectrum. It is thus possible to recognize the effect of interstellar reddening in the discrepancy that may result from the comparison of the temperatures obtained by normalizing at the V-magnitude or at some point in the ultraviolet range. We have not tested the effect of extremely large extinction coefficients ($E_{B-V} \gg 0.1$) as in L86 because the effect of the resultant 2200 Å depression on the quality of the fit is catastrophic as we will see. The effect of interstellar reddening on the resultant effective temperature is easy to estimate. The application of an extinction coefficient $E_{B-V} = 0.01$ to a synthetic spectrum results in a 5% reduction of the FUV flux normalized at the V magnitude. Such an effect translates to a 500 K increase of the fitted temperature for a model at 25,000 K.

The largest contribution to the error estimate comes from a 5%–10% error assigned to the normalization constant applied to the ultraviolet flux, which is obtained using the optical pivot (V Johnson or MCSP). Added to this basic error estimate are the intrinsic theoretical uncertainties and an error defined by the extent of the discrepancy between the results obtained using different normalization procedures. All *IUE* SWP and LWR images have been corrected for the time-dependent sensitivity degradation of the cameras and the residual distortions have been removed using the formalism presented by Finley, Basri, & Bowyer (1990). Apparently all *IUE* LWP exposures suffer from a calibration problem, and for most of it, they do not permit the exploration of the effect of reddening in the corresponding stars. We present, in the following, a brief description of the individual analyses from our sample of eleven DB white dwarfs presented in Table 3.

1. WD 0112+104 (PG; Fig. 6). The uncertainty on the temperature is rather large as the fit found when normalizing the flux at 1850 Å ($T_{\rm eff}$ = 24,700 K) is much cooler than that found using the normalization at $V_{\rm MCSP}$ ($T_{\rm eff}$ = 27,700 K). This is why we propose a much larger uncertainty than that quoted in L86. The range of acceptable solutions is set by subtracting the uncertainty on the models (400 K) from the lowest temperature we obtained and by adding, to the highest temperature, the

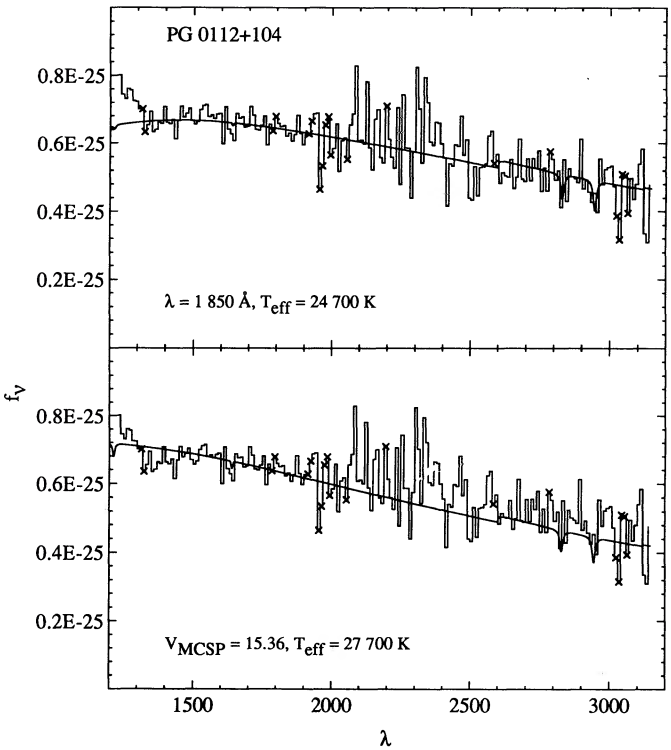

FIG. 6.—(*a*) (*Top*). Ultraviolet spectrum of the star PG 0112+104 and the synthetic spectrum of a model at $T_{\rm eff}$ = 24,700 K and log g = 8 normalized to the observed spectrum at λ = 1850 Å. The *IUE* spectrum is displayed with 10 Å wide bins, while the synthetic spectrum has been convolved with a 7 Å wide Gaussian. Crosses indicate bins excluded from the analysis. (*b*) (*bottom*). Same as Fig. 6*a* but with a model at $T_{\rm eff}$ = 27,700 K and normalized at $V_{\rm MCSP}$.

TABLE 3

TEMPERATURES FOR THE HOT DB WHITE DWARFS ($T_{\rm eff}$ > 20,000 K)

WD #	Name[a]	T_W[b]	T_K[c]	$T_{\rm opt}$[d]	$T_{\rm eff}$[e]	mag[f]	*IUE*[g]
0112+104	PG (S)	30 ± 1	29 ± 2	28.9 ± 0.6	24.3–29.3	$V_{\rm mcsp}$ = 15.36	swp 18510 lwr 13655
1645+325	GD 358 (V)	28 ± 1	27^{+1}_{-2}	24.6 ± 0.5	24.0 ± 1.0	V = 13.62	swp 25310 lwr 10668
1654+160	PG (V)	26^{+2}_{-1}	25 ± 2	...	21.5:	...	swp 22355 lwp 02846
1115+158	PG (V)	26 ± 2	25 ± 2	...	22.5:	...	swp 23033 lwp 03376
0308−565	BPM 17088	26 ± 1	23^{+1}_{-2}	...	21.5 ± 0.5	V = 14.07	swp 07459 lwr 06467
					E_{B-V} = 0.02		
1542+182	GD 190 (S)	26 ± 1	23^{+2}_{-1}	22.7 ± 1	23.0 ± 1.5	V = 14.70	swp 03725 lwr 01588
					$E_{B-V} \leq$ 0.02		
1351+489	PG (V)	25 ± 2	24^{+1}_{-2}	...	22.0:	...	swp 25299 lwp 05408
0100−068	BPM 70524	25^{+1}_{-2}	22 ± 1	19–23	22.0 ± 1.0	V = 13.92	swp 07488 lwr 06529
					E_{B-V} = 0.04		
1456+103	PG (V)	24 ± 3	23^{+3}_{-1}	...	22.5:	...	swp 25311 lwp 05416
0853+163	LB 8827 (S)	22^{+3}_{-2}	22^{+1}_{-2}	...	21.0 ± 1.0	$V_{\rm mcsp}$ = 15.81	swp 23030 lwp 03375
1445+152	PG	...	...	23[h]	20.5 ± 1.0	...	swp 19548 lwr 15584

[a] The label (S) refers to a stable DB star, while the label (V) refers to a DBV star.
[b] Temperature from L86 obtained with Wesemael (1981) models.
[c] Temperature from L86 obtained with Koester (1980) models.
[d] Optical temperatures compiled by L86.
[e] Temperature determination from the present study and the associated extinction coefficient.
[f] Magnitude used in the determination of the normalization constant.
[g] *IUE* short- and long-wavelength exposures in the temperature determinations.
[h] Temperature from Wegner & Nelan (1987) obtained using optical and *IUE* data.

uncertainty on the models and the effect of a 10% error on the normalization constant derived using the $V_{MCSP} = 15.36$ pivot (1600 K). No reddening has been added because then the discrepancy would be worse, as would be the statistical quality of the fit around the 2200 Å "bump" in the extinction law. We have not used the new spectrophotometric measurements of Greenstein & Liebert (1990) because the large difference between their results for this star and those published by Greenstein et al. (1977) has not been explained; the $V_{MCSP} =$ 15.51 magnitude obtained by Greenstein & Liebert (1990) would raise the temperature of this star to $T_{eff} > 30{,}000$ K.

2. WD 1645+325 (GD 358; Fig. 7). A normalization at 1850 and 2780 Å provides a consistent fit at 23,500 K, while the normalization at $V_{Johnson} = 13.62$ gives $T_{eff} = 24{,}200$ K. From the absence of flux depression at 2200 Å and because of the agreements between the two derived temperatures the extinction coefficient is assumed to be small. The total error is set by the effect of a 5% error on the optical normalization constant in addition to the uncertainty on the models. We note the presence in the long-wavelength exposure of two members of the He I 2^3S line series $\lambda\lambda$ 2829 and 2945 Å, apparently consistent with the model.

3. WD 1542+182 (GD 190; Fig. 8). The best solutions obtained for this star are apparently less satisfactory than for GD 358 or BPM 17088. The models do not reproduce the shape of the *IUE* exposures for any value of $E_{B-V} \leq 0.02$. One possibility is that GD 190 is reddened in a way not well-described by the Seaton (1979) law. We obtained $T_{eff} = 23{,}400$ and 23,100 K when normalizing at the V magnitude and $\lambda = 2875$ Å, respectively ($E_{B-V} = 0.01$). In the total error we have added the uncertainty on the models, and the effects of an unknown amount of interstellar reddening and of a 5% uncertainty on the optical normalization constant ($V = 14.7$). Our new temperatures for this nonpulsating DB star and for the group of DBV stars, may well place GD 190 *above* the DB instability strip instead of below it.

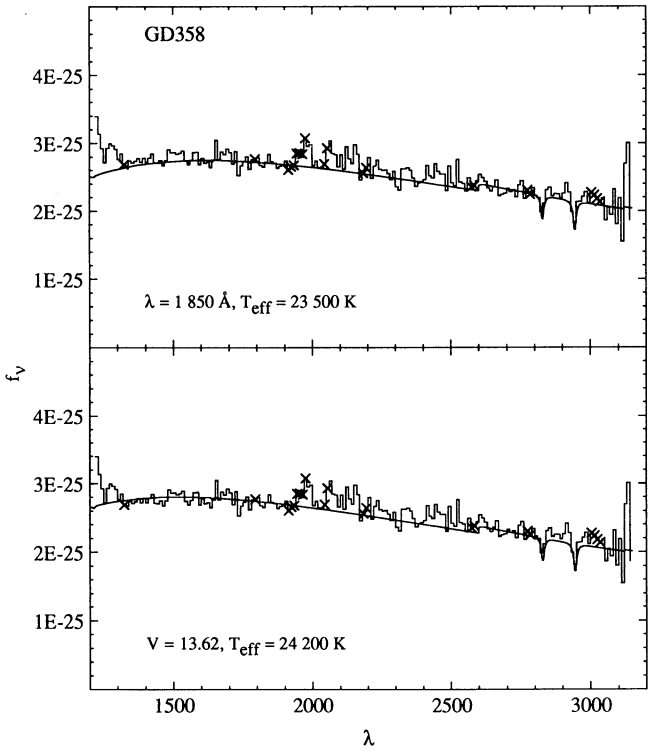

FIG. 7.—(*a*) (*Top*). Ultraviolet spectrum of the star GD 358 and the synthetic spectrum of a model at $T_{eff} = 23{,}500$ K and log $g = 8$ normalized to the observed spectrum at $\lambda = 1850$ Å. (*b*) (*Bottom*). Same as Fig. 7*a* but with a model at $T_{eff} = 24{,}200$ K and normalized at V.

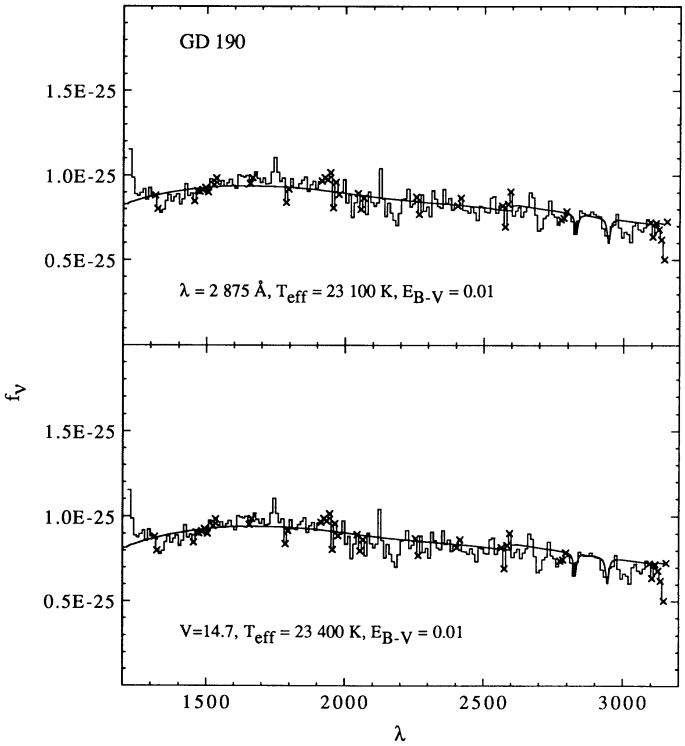

FIG. 8.—(*a*) (*Top*). Ultraviolet spectrum of the star GD 190 and the synthetic spectrum of a model at $T_{eff} = 23{,}100$ K and log $g = 8$ normalized to the observed spectrum at $\lambda = 2875$ Å. The effect of interstellar reddening ($E_{B-V} = 0.01$) is applied to the model. (*b*) (*Bottom*). Same as Fig. 8*a* but with a model at $T_{eff} = 23{,}400$ K and normalized at V.

4. WD 1456+103 (PG; Fig. 9*a*). Due to the absence of optical photometry and to the low quality of the LWP exposure we can only derive an uncertain $T_{eff} = 22{,}500$ K. For the same reason it is not possible to explore the effect of interstellar reddening. The range 1950–2400 Å is excluded from the analysis.

5. WD 1115+158 (PG; Fig. 9*b*). The analysis of this star is similar to that of PG 1456+103 and leads to the same conclusion with a temperature of $T_{eff} = 22{,}500$ K. The entire long-wavelength range (LWP) has been excluded from the analysis.

6. WD 0100−068 (BPM 70524; Fig. 10). The inclusion of a small amount of reddening improves greatly the fit (E_{B-V}) = 0.04). The normalizations at 1850 Å and at $V = 13.92$ provide a unique solution at $T_{eff} = 22{,}000$ K. The error is set by a 5% uncertainty on the V-magnitude and by the uncertainty on the models.

7. WD 1351+489 (PG; Fig. 11*a*). Again the low quality of the data limits us to an uncertain T_{eff} of about 22,000 K.

8. WD 1654+160 (PG; Fig. 11*b*). Due to the low quality of the *IUE* exposures in this case and to the absence of optical photometric measurements, we have estimated a minimum error by normalizing at 1850 Å and 2700 Å. We have excluded from the analysis the wavelength range 1950–2400 Å. The effective temperature is found between 20,500 K and 22,500 K.

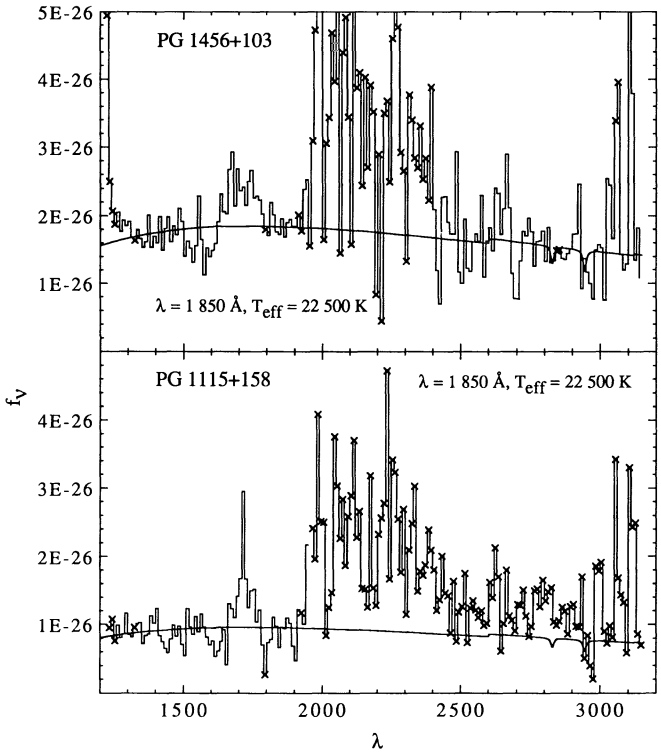

FIG. 9.—(*a*) (*Top*). Ultraviolet spectrum of the star PG 1456+103 and the synthetic spectrum of a model at $T_{\rm eff}$ = 22,500 K and log g = 8 normalized to the observed spectrum at λ = 1850 Å. (*b*) (*Bottom*). Ultraviolet spectrum of the star PG 1115+158 and the synthetic spectrum of a model at $T_{\rm eff}$ = 22,500 K and log g = 8 normalized to the observed spectrum at λ = 1850 Å.

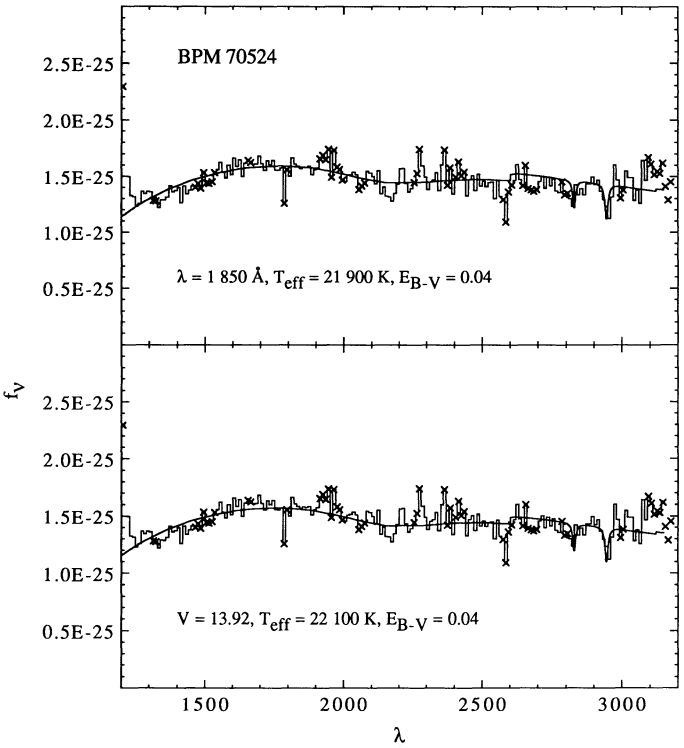

FIG. 10.—(*a*) (*Top*). Ultraviolet spectrum of the star BPM 70524 and the synthetic spectrum of a model at $T_{\rm eff}$ = 21,900 K and log g = 8 normalized to the observed spectrum at λ = 1850 Å. The effect of interstellar reddening (E_{B-V} = 0.04) is applied to the model. (*b*) (*Bottom*). Same as Fig. 10*a* but with a model at $T_{\rm eff}$ = 22,100 K and normalized at V.

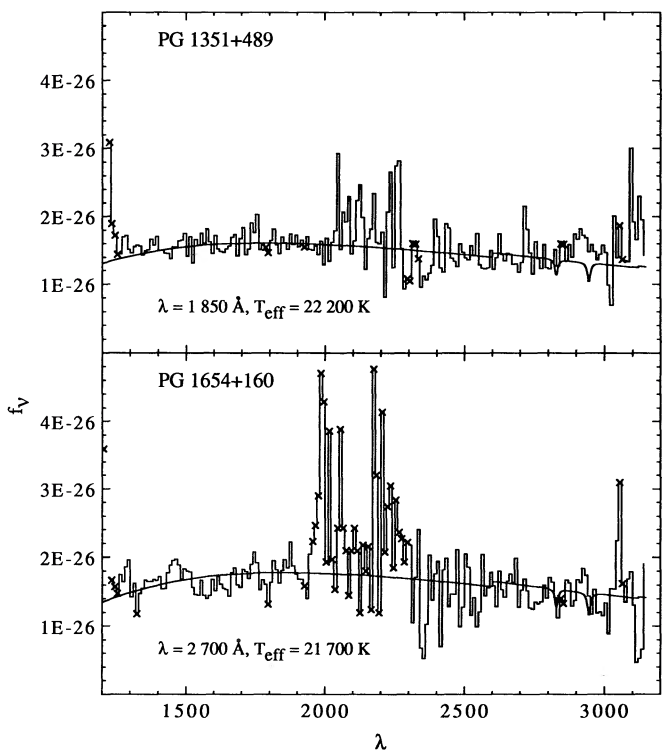

FIG. 11.—(*a*) (*Top*). Ultraviolet spectrum of the star PG 1351+489 and the synthetic spectrum of a model at $T_{\rm eff}$ = 22,200 K and log g = 8 normalized to the observed spectrum at λ = 1850 Å. (*b*) (*Bottom*). Ultraviolet spectrum of the star PG 1654+160 and the synthetic spectrum of a model at $T_{\rm eff}$ = 21,700 K and log g = 8 normalized to the observed spectrum at λ = 2700 Å.

9. WD 0308−565 (BPM) 17088; Fig. 12). The exceptionally well determined V (and y) magnitude of that star encourages us to use a 5% error instead of 10% on the normalization constant. The normalization at 1850 and 2900 Å gives $T_{\rm eff}$ = 21,800 and 21,300 K, respectively, with the best χ^2 value at E_{B-V} = 0.02. Higher values of E_{B-V} cause a dramatic increase in the χ^2 value. We obtain a consistent solution at $T_{\rm eff}$ = 21,800 K if normalizing at the magnitude V. The parameters of that star are thus exceptionally well-determined. The lines He I $\lambda\lambda$2829, 2945 Å are clearly detected.

10. WD 0853+163 (LB 8827; Fig. 13). The two different normalization procedures ($V_{\rm MCSP}$ = 15.81 and λ = 1850 Å) are consistent with a unique solution at $T_{\rm eff}$ = 21,000 K. The 1950–2400 Å range has been excluded.

11. WD 1445+152 (PG; Fig. 14). The normalization at λ = 1850 Å gives a solution at $T_{\rm eff}$ = 20,500 K.

In Figure 15 we show the Wesemael (1981) and Koester (1980) temperatures from L86 and the new temperatures from this paper.

What is the statistical significance of the new temperature estimates? Each new temperature is lower than those for WL 86 (Wesemael 1981 in L86) and also those for KL 86 (Koester 1980 in L86). Let us focus on the differences to the WL 86 determinations. Excluding the individual temperature estimates that are too uncertain, i.e., those for which we do not give error estimates, then for each object (i) we calculate the size of the temperature decrease

$$\Delta T_i = T_{\rm WL\,86} - T_{\rm us} \quad (4)$$

as well as the associated error. This error is calculated by error propagation techniques

$$\sigma(\Delta T_i) = [\sigma^2(T_{\rm WL\,86}) + \sigma^2(T_{\rm us})]^{1/2} . \quad (5)$$

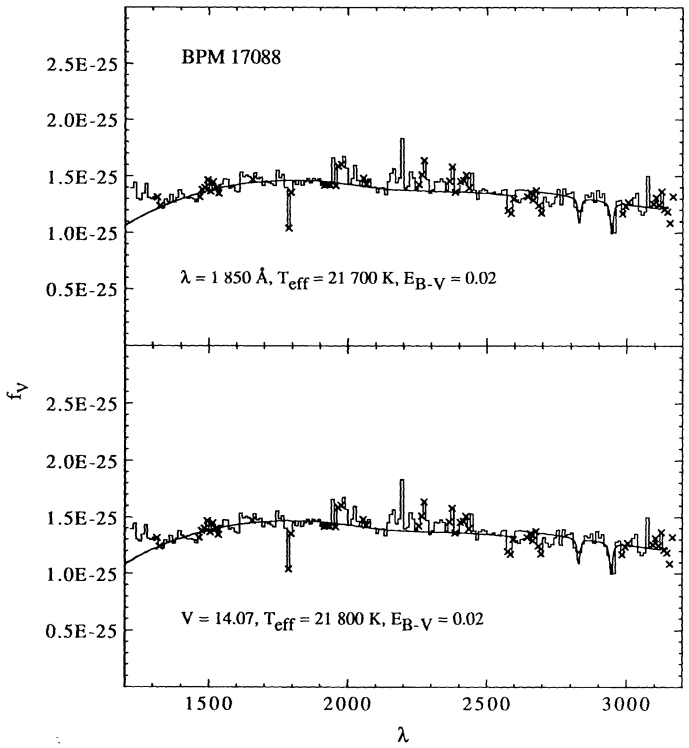

FIG. 12.—(*a*) (*Top*). Ultraviolet spectrum of the star BPM 17088 and the synthetic spectrum of a model at $T_{\rm eff}$ = 21,700 K and log g = 8 normalized to the observed spectrum at λ = 1850 Å. The effect of interstellar reddening (E_{B-V}) = 0.02) is applied to the model. (*b*) (*Bottom*). Same as Fig. 12*a* but with a model at $T_{\rm eff}$ = 21,800 K and normalized at V.

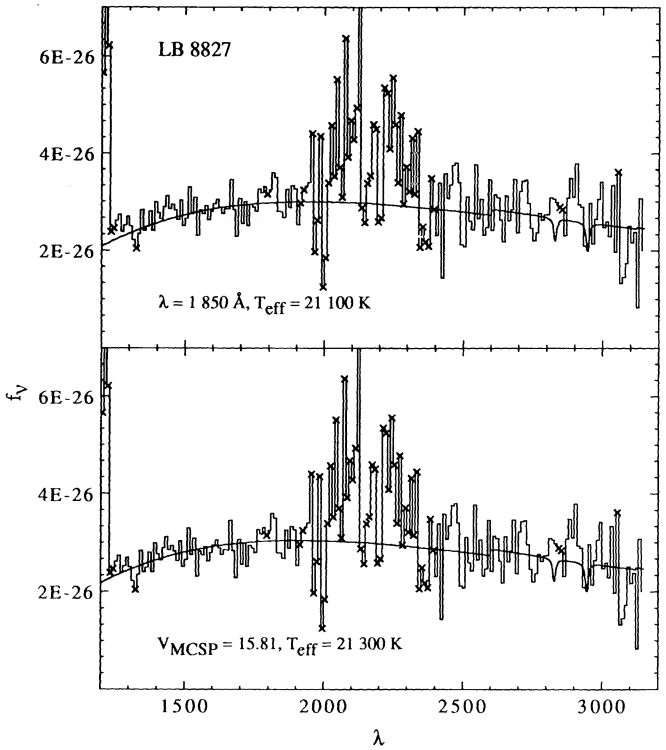

FIG. 13.—(*a*) (*Top*). Ultraviolet spectrum of the star LB 8827 and the synthetic spectrum of a model at $T_{\rm eff}$ = 21,100 K and log g = 8 normalized to the observed spectrum at λ = 1850 Å. (*b*) (*Bottom*). Same as Fig. 13*a* but with a model at $T_{\rm eff}$ = 21,300 K and normalized at $V_{\rm MCSP}$.

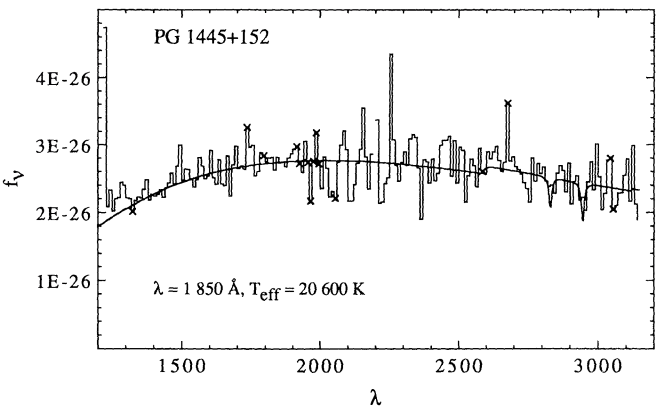

FIG. 14.—Ultraviolet spectrum of the star PG 1445+152 and the synthetic spectrum of a model at $T_{\rm eff}$ = 20,600 K and log g = 8 normalized to the observed spectrum at λ = 1850 Å.

For each object the significance of the temperature deviation is expressed as

$$z_i = \frac{\Delta T_i}{\sigma(\Delta T_i)} . \tag{6}$$

The significance of the mean temperature deviation for the whole sample is then

$$\frac{\sum z_i}{n^{1/2}} \tag{7}$$

by the central limit theorem.

Performing this calculation for the six objects that have error estimates, we get an overall significance for the temperature deviation of 4.4, i.e., our new temperature determination has found a different result than that published before significant to the 4 or 5 σ level. The similarly calculated significance level for our temperature difference vis-à-vis KL 86 gives 1.3, which is not a significant difference.

The overall lowering of the effective temperature is due to simple physical effects; in the case of WL 86 it is due to the

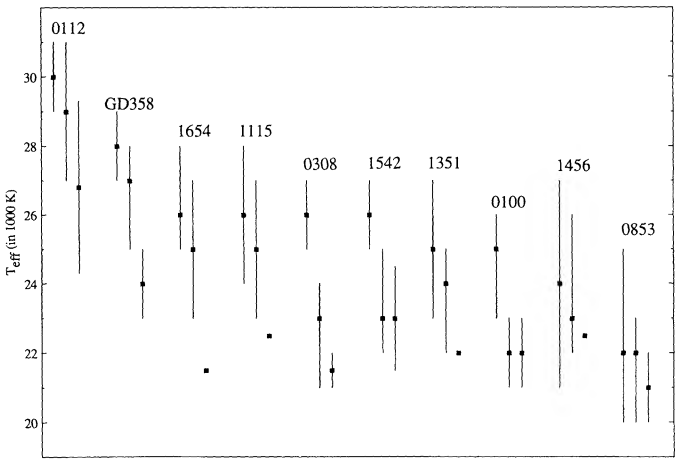

FIG. 15.—Temperatures of the DB and DBV stars from Liebert et al. (1986) using models of Wesemael and Koester, and our determinations. In each group of three temperatures the left one is that due to Wesemael (1981) in L86, the middle is due to Koester (1980) in L86 and the right one is our determination. Each star is labeled either by its most usual denomination or by the first four digits of the WD number.

much cooler W81 models being used—to achieve the same flux at a certain wavelength the W81 models need to be hotter, and therefore the stars that are fitted using those models will have a hotter effective temperature. In the case of the KL 86 models we believe that they give slightly higher temperatures (not statistically significant) than ours because ours are both hydrogen and helium line blanketed, while the KL 86 models appear to be only hydrogen line blanketed, and blanketing forces models to become slightly hotter in order to output the same flux as a cooler unblanketed model.

While our $T_{\rm eff}$ determinations individually are not all significantly different from the previous determinations, *it is significant that our determinations, taken as a whole, are always lower than WL 86*. It is also worth noting that the KL 86 temperatures are lower than WL 86 in all cases, and agree with our values in two cases: 1542+182 and 0100−068. The largest discrepancies between our solutions and those found by WL 86 and KL 86 occur at 25,000 K, where the He I blanketing effect is at its maximum.

We feel that the analysis of the effective temperature of the DB and DBV stars has been improved over previous investigations by the use of an optical pivot for the calculation of a normalization constant (this allows the combination of slope and absolute-level information to enter the fitting procedure at the same time) and by the recent availability of tables of the *IUE* time-dependent degradation of the short- and long-wavelength cameras (Bohlin & Grillmair 1988). In most cases the systematic lowering of the effective temperature finds its roots in the previously stated differences between our models and those of earlier investigations.

5. IMPLICATIONS OF LOWER TEMPERATURES FOR THE DBV STARS

The result of the present re-analysis is that the variable DBV stars have significantly lower temperatures, inferred from *IUE* data, than previously reported. The upper temperature limit on the instability strip that our new results provides has some impact on the choice of the mixing-length theory that gives the best fit between theoretical predictions of the placement of the instability strip and the observations. Four of the DBV stars have effective temperatures near 22,000 K, and since the instability strip is predicted to be 3000 K wide (Winget et al. 1983), its upper limit should fall at or near 25,000 K. This is where we find GD 358, the hottest DBV. From the theoretical considerations of Fontaine et al. (1984) (see their Fig. 2), it is then evident that ML 3 no longer produces the pulsations at the observed temperature range and that ML 2 is a better candidate.

Our best fitting effective temperature for GD 358 is 24,000 ± 1000 K. Sion et al. (1988) have presented interesting evidence of the He II line at 1640 Å, as well as ionized carbon. What effective temperature does a He II λ1640 line indicate? Using their published spectrum we estimate that the equivalent width of He II λ1640 is ≤0.25 Å. With equivalent widths of the line, measured from our grid (see Fig. 16), we get a temperature below 28,000 K. Sion et al. (1988) found that such a strong line might indicate a higher temperature, in the 30,000 K range or into the DB gap itself. In comparing the shape of the λ1640 feature in the co-added spectrum of Sion et al. (1988) with our model profiles (Fig. 17) it is apparent that the 30,000 K line-profile does not have any core to match the observed dip, nor does the 35,000 K model and it has in addition wide wings that do not match what is seen in the observed data. Low-dispersion data, while less noisy, have a resolution of 7 Å FWHM, and it is not possible to determine equivalent widths of features that are of the order of 0.25 Å.

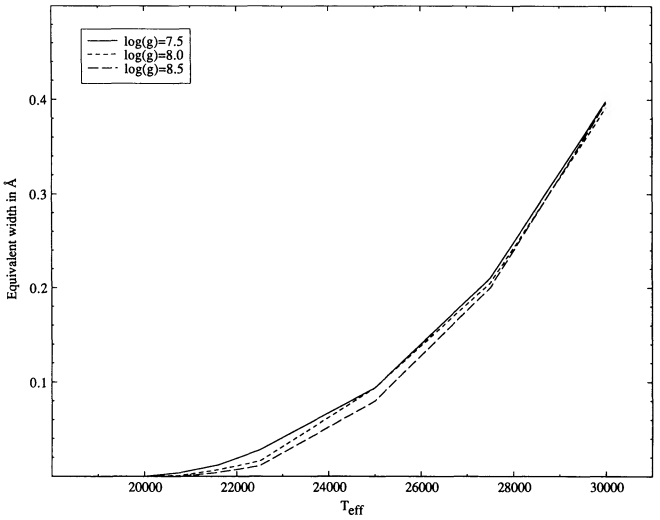

FIG. 16.—Predicted equivalent widths of He II 1640 as a function of temperature and gravity.

Incidentally, we have modeled the C II lines that Sion et al. (1988) report in the high-resolution SWP images, using 25,000 K/log g = 8 models with varying amounts of carbon. We estimate that the carbon abundance in GD 358 [n(C)/n(tot)] is between 10^{-4} and 10^{-5} which is between 0.1 and 0.01 of the solar abundance. This detection, if confirmed, presents an interesting theoretical challenge as radiative support on carbon cannot, at this temperature, account for the abundance we inferred, not to mention the dredge-up process, which is inactive at 25,000 K (Pelletier et al. 1986). It is also difficult to explain by accretion the presence of carbon and simultaneously the absence of hydrogen.

6. CONCLUSIONS

We have calculated a new grid of helium-dominated models and redetermined the effective temperatures of some of the DB

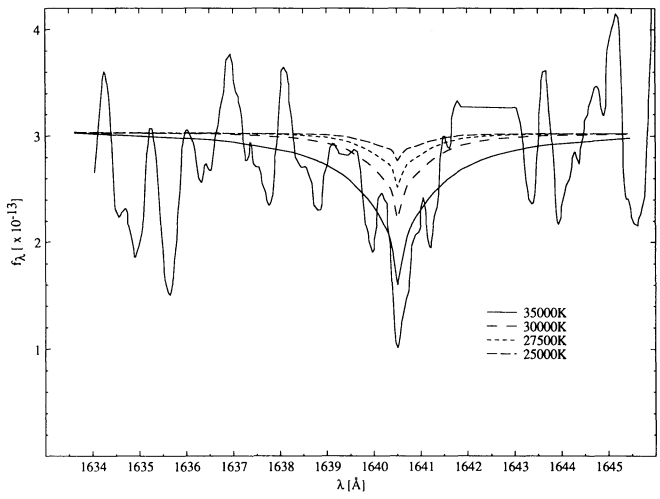

FIG. 17.—The co-added *IUE* high-dispersion spectrum for GD 358 from Sion et al. (1988), and synthetic spectra of the He II λ1640 line. The model line profiles are unsmoothed, and the *IUE* image has been digitized from Sion et al. (1988; Fig. 1). None of our models can fit the sharp-line core without developing strong wings, which are unobserved.

TABLE 4

THE MODEL STRUCTURES

TEFF=19000. LOG(G)= 8.00 ML2. PURE He				TEFF=20000. LOG(G)= 8.00 ML2. PURE He			
M	TEMP	NE	NTOT	M	TEMP	NE	NTOT
7.768E-07	1.302E+04	1.139E+13	4.321E+13	7.768E-07	1.335E+04	1.333E+13	4.216E+13
1.104E-06	1.363E+04	1.860E+13	5.867E+13	1.104E-06	1.393E+04	2.060E+13	5.740E+13
1.546E-06	1.375E+04	2.481E+13	8.148E+13	1.546E-06	1.404E+04	2.760E+13	7.975E+13
2.137E-06	1.388E+04	3.274E+13	1.115E+14	2.137E-06	1.418E+04	3.660E+13	1.092E+14
2.920E-06	1.402E+04	4.282E+13	1.508E+14	2.920E-06	1.432E+04	4.813E+13	1.477E+14
3.934E-06	1.415E+04	5.522E+13	2.013E+14	3.934E-06	1.446E+04	6.249E+13	1.970E+14
5.258E-06	1.428E+04	7.035E+13	2.667E+14	5.258E-06	1.460E+04	8.030E+13	2.608E+14
6.990E-06	1.439E+04	8.844E+13	3.518E+14	6.990E-06	1.473E+04	1.021E+14	3.437E+14
9.274E-06	1.448E+04	1.096E+14	4.640E+14	9.274E-06	1.483E+04	1.283E+14	4.528E+14
1.222E-05	1.453E+04	1.329E+14	6.091E+14	1.222E-05	1.491E+04	1.581E+14	5.936E+14
1.608E-05	1.455E+04	1.581E+14	8.005E+14	1.608E-05	1.495E+04	1.910E+14	7.791E+14
2.122E-05	1.454E+04	1.847E+14	1.057E+15	2.122E-05	1.495E+04	2.268E+14	1.028E+15
2.813E-05	1.449E+04	2.126E+14	1.406E+15	2.813E-05	1.491E+04	2.654E+14	1.367E+15
3.726E-05	1.445E+04	2.448E+14	1.867E+15	3.726E-05	1.492E+04	3.181E+14	1.808E+15
4.967E-05	1.443E+04	2.861E+14	2.493E+15	4.967E-05	1.496E+04	3.879E+14	2.404E+15
6.674E-05	1.445E+04	3.440E+14	3.344E+15	6.674E-05	1.503E+04	4.802E+14	3.216E+15
9.046E-05	1.450E+04	4.219E+14	4.517E+15	9.046E-05	1.511E+04	5.996E+14	4.336E+15
1.236E-04	1.457E+04	5.216E+14	6.148E+15	1.236E-04	1.515E+04	7.303E+14	5.912E+15
1.704E-04	1.459E+04	6.293E+14	8.462E+15	1.704E-04	1.519E+04	8.981E+14	8.125E+15
2.373E-04	1.462E+04	7.697E+14	1.176E+16	2.373E-04	1.524E+04	1.111E+15	1.128E+16
3.339E-04	1.467E+04	9.486E+14	1.649E+16	3.339E-04	1.532E+04	1.397E+15	1.579E+16
4.742E-04	1.472E+04	1.179E+15	2.334E+16	4.742E-04	1.532E+04	1.696E+15	2.242E+16
6.793E-04	1.478E+04	1.489E+15	3.328E+16	6.793E-04	1.532E+04	2.056E+15	3.212E+16
9.805E-04	1.480E+04	1.825E+15	4.797E+16	9.805E-04	1.533E+04	2.511E+15	4.634E+16
1.424E-03	1.480E+04	2.206E+15	6.970E+16	1.424E-03	1.534E+04	3.077E+15	6.725E+16
2.076E-03	1.480E+04	2.693E+15	1.016E+17	2.076E-03	1.536E+04	3.800E+15	9.792E+16
3.033E-03	1.481E+04	3.293E+15	1.483E+17	3.033E-03	1.540E+04	4.729E+15	1.427E+17
4.427E-03	1.484E+04	4.052E+15	2.161E+17	4.427E-03	1.545E+04	5.933E+15	2.075E+17
6.429E-03	1.487E+04	5.011E+15	3.132E+17	6.429E-03	1.552E+04	7.497E+15	3.000E+17
9.252E-03	1.492E+04	6.228E+15	4.491E+17	9.252E-03	1.561E+04	9.556E+15	4.292E+17
1.312E-02	1.499E+04	7.775E+15	6.339E+17	1.312E-02	1.575E+04	1.236E+16	6.033E+17
1.822E-02	1.508E+04	9.767E+15	8.749E+17	1.822E-02	1.593E+04	1.625E+16	8.282E+17
2.472E-02	1.522E+04	1.241E+16	1.176E+18	2.472E-02	1.622E+04	2.234E+16	1.104E+18
3.232E-02	1.539E+04	1.585E+16	1.521E+18	3.232E-02	1.645E+04	2.896E+16	1.423E+18
4.057E-02	1.561E+04	2.030E+16	1.882E+18	4.057E-02	1.782E+04	6.384E+16	1.649E+18
5.057E-02	1.590E+04	2.680E+16	2.303E+18	5.057E-02	2.010E+04	1.710E+17	1.823E+18
5.855E-02	1.611E+04	3.266E+16	2.632E+18	5.855E-02	2.117E+04	2.559E+17	2.004E+18
6.906E-02	1.779E+04	8.264E+16	2.812E+18	6.906E-02	2.196E+04	3.459E+17	2.278E+18
7.847E-02	1.907E+04	1.508E+17	2.981E+18	7.847E-02	2.260E+04	4.340E+17	2.515E+18
8.674E-02	1.973E+04	2.033E+17	3.184E+18	8.674E-02	2.297E+04	4.999E+17	2.735E+18
9.936E-02	2.053E+04	2.857E+17	3.506E+18	9.936E-02	2.357E+04	6.143E+17	3.053E+18
1.178E-01	2.128E+04	3.936E+17	4.010E+18	1.178E-01	2.414E+04	7.598E+17	3.534E+18
1.464E-01	2.219E+04	5.703E+17	4.779E+18	1.464E-01	2.502E+04	1.009E+18	4.239E+18
1.985E-01	2.321E+04	8.701E+17	6.194E+18	1.985E-01	2.599E+04	1.416E+18	5.531E+18
2.708E-01	2.433E+04	1.330E+18	8.062E+18	2.708E-01	2.719E+04	2.026E+18	7.214E+18
3.557E-01	2.515E+04	1.827E+18	1.024E+19	3.557E-01	2.808E+04	2.695E+18	9.176E+18

and DBV white dwarfs, using *IUE* data corrected with the best knowledge of the time-dependent camera degradation available. For most of the stars we analyzed, model atmospheres reproduce satisfactorily the observations with a minimum of free parameters. In some cases, a small amount of reddening was inferred, although for most cases the absence of any depression at 2150 Å rules out the presence of significant reddening effect. We have found an overall significant lowering of the effective temperatures over previous investigations.

With these new, lower effective temperatures, the hottest DBV star is so cool that there is no longer support for the ML 3 convective mixing theory, a hypothesis that was put forward on the basis of the earlier, higher temperatures. Unfortunately, the uncertainties on the effective temperature of the DBV and surrounding DB stars remain so large that we have not been able to strictly establish the existence of an instability strip, though all DBV stars seem to cluster in the 22,000–25,000 K band. Both BPM 17088 and BPM 70524 have temperatures that make them likely pulsators, though the uncertainty on their temperatures are large. Even if it is premature to predict if

TABLE 4—*Continued*

TEFF=20800. LOG(G)= 8.00 ML2. PURE He				TEFF=21600. LOG(G)= 8.00 ML2. PURE He			
M	TEMP	NE	NTOT	M	TEMP	NE	NTOT
7.768E-07	1.359E+04	1.455E+13	4.142E+13	7.768E-07	1.383E+04	1.546E+13	4.067E+13
1.104E-06	1.414E+04	2.173E+13	5.656E+13	1.104E-06	1.435E+04	2.253E+13	5.574E+13
1.546E-06	1.425E+04	2.922E+13	7.862E+13	1.546E-06	1.446E+04	3.043E+13	7.747E+13
2.137E-06	1.438E+04	3.889E+13	1.076E+14	2.137E-06	1.459E+04	4.063E+13	1.061E+14
2.920E-06	1.453E+04	5.133E+13	1.456E+14	2.920E-06	1.474E+04	5.378E+13	1.435E+14
3.934E-06	1.468E+04	6.694E+13	1.942E+14	3.934E-06	1.489E+04	7.036E+13	1.914E+14
5.258E-06	1.482E+04	8.650E+13	2.569E+14	5.258E-06	1.504E+04	9.130E+13	2.531E+14
6.990E-06	1.496E+04	1.108E+14	3.384E+14	6.990E-06	1.519E+04	1.176E+14	3.333E+14
9.274E-06	1.509E+04	1.406E+14	4.452E+14	9.274E-06	1.533E+04	1.504E+14	4.383E+14
1.222E-05	1.519E+04	1.754E+14	5.829E+14	1.222E-05	1.544E+04	1.896E+14	5.732E+14
1.608E-05	1.526E+04	2.156E+14	7.635E+14	1.608E-05	1.553E+04	2.360E+14	7.503E+14
2.122E-05	1.529E+04	2.614E+14	1.005E+15	2.122E-05	1.559E+04	2.915E+14	9.860E+14
2.813E-05	1.530E+04	3.161E+14	1.331E+15	2.813E-05	1.563E+04	3.598E+14	1.303E+15
3.726E-05	1.532E+04	3.845E+14	1.761E+15	3.726E-05	1.569E+04	4.471E+14	1.719E+15
4.967E-05	1.540E+04	4.783E+14	2.337E+15	4.967E-05	1.580E+04	5.647E+14	2.277E+15
6.674E-05	1.549E+04	6.020E+14	3.120E+15	6.674E-05	1.591E+04	7.172E+14	3.038E+15
9.046E-05	1.555E+04	7.456E+14	4.213E+15	9.046E-05	1.597E+04	8.907E+14	4.104E+15
1.236E-04	1.560E+04	9.207E+14	5.739E+15	1.236E-04	1.604E+04	1.116E+15	5.584E+15
1.704E-04	1.566E+04	1.144E+15	7.881E+15	1.704E-04	1.607E+04	1.381E+15	7.680E+15
2.373E-04	1.571E+04	1.421E+15	1.094E+16	2.373E-04	1.607E+04	1.686E+15	1.070E+16
3.339E-04	1.571E+04	1.725E+15	1.539E+16	3.339E-04	1.607E+04	2.061E+15	1.504E+16
4.742E-04	1.571E+04	2.099E+15	2.186E+16	4.742E-04	1.609E+04	2.536E+15	2.135E+16
6.793E-04	1.572E+04	2.573E+15	3.129E+16	6.793E-04	1.610E+04	3.129E+15	3.056E+16
9.805E-04	1.574E+04	3.164E+15	4.513E+16	9.805E-04	1.613E+04	3.890E+15	4.403E+16
1.424E-03	1.576E+04	3.923E+15	6.543E+16	1.424E-03	1.618E+04	4.879E+15	6.376E+16
2.076E-03	1.580E+04	4.906E+15	9.516E+16	2.076E-03	1.624E+04	6.176E+15	9.262E+16
3.033E-03	1.587E+04	6.191E+15	1.385E+17	3.033E-03	1.632E+04	7.887E+15	1.346E+17
4.427E-03	1.595E+04	7.879E+15	2.011E+17	4.427E-03	1.643E+04	1.018E+16	1.952E+17
6.429E-03	1.605E+04	1.013E+16	2.902E+17	6.429E-03	1.658E+04	1.337E+16	2.809E+17
9.252E-03	1.620E+04	1.326E+16	4.137E+17	9.252E-03	1.679E+04	1.796E+16	3.992E+17
1.312E-02	1.640E+04	1.773E+16	5.792E+17	1.312E-02	1.710E+04	2.514E+16	5.557E+17
1.822E-02	1.672E+04	2.471E+16	7.894E+17	1.822E-02	1.745E+04	3.526E+16	7.563E+17
2.472E-02	1.700E+04	3.330E+16	1.053E+18	2.472E-02	1.952E+04	9.470E+16	9.170E+17
3.232E-02	1.908E+04	9.400E+16	1.227E+18	3.232E-02	2.227E+04	2.313E+17	1.051E+18
4.057E-02	2.174E+04	2.375E+17	1.352E+18	4.057E-02	2.385E+04	3.528E+17	1.232E+18
5.057E-02	2.268E+04	3.354E+17	1.615E+18	5.057E-02	2.502E+04	4.758E+17	1.464E+18
5.855E-02	2.362E+04	4.386E+17	1.795E+18	5.855E-02	2.590E+04	5.752E+17	1.638E+18
6.906E-02	2.419E+04	5.371E+17	2.067E+18	6.906E-02	2.665E+04	6.907E+17	1.877E+18
7.847E-02	2.485E+04	6.429E+17	2.287E+18	7.847E-02	2.741E+04	7.995E+17	2.073E+18
8.674E-02	2.518E+04	7.186E+17	2.495E+18	8.674E-02	2.785E+04	8.862E+17	2.256E+18
9.936E-02	2.584E+04	8.530E+17	2.785E+18	9.936E-02	2.871E+04	1.026E+18	2.506E+18
1.178E-01	2.640E+04	1.022E+18	3.232E+18	1.178E-01	2.948E+04	1.210E+18	2.893E+18
1.464E-01	2.741E+04	1.312E+18	3.869E+18	1.464E-01	3.094E+04	1.492E+18	3.427E+18
1.985E-01	2.847E+04	1.791E+18	5.048E+18	1.985E-01	3.264E+04	1.978E+18	4.403E+18
2.708E-01	2.992E+04	2.470E+18	6.556E+18	2.708E-01	3.509E+04	2.593E+18	5.591E+18
3.557E-01	3.098E+04	3.213E+18	8.315E+18	3.557E-01	3.734E+04	3.266E+18	6.900E+18

a particular DB white dwarf will be detected as a variable star or not, on the basis of a temperature obtained from optical or ultraviolet flux measurements, these two stars are the most logical candidates for such a prediction.

In having found a cooler temperature for the hottest DB star below the DB "gap" (PG 0112+104) we have widened the DB gap somewhat. Instead of having the red edge at 30,000 ± 1000 K (L86) it is now at 27,500 ± 2000 K. This makes the reality of the gap easier to accept, and it is less probable that it is due to small-number statistics, as suggested in D'Antona (1988).

For the star GD 358 we find that the He II line at 1640 Å, discovered by Sion et al. (1988), does not support their suggestion that GD 358 is as hot as 30,000 K or more, because the observed feature does not match the morphology of the theoretical line profiles. We find that the C II lines identified by Sion et al. (1988) indicates a carbon abundance in GD 358 of roughly log $[n(\mathrm{C})/n(\mathrm{tot})] = -4$ to -5. It is interesting to note that the present difficulty in explaining the presence of photospheric C II λ1334 and He II λ 1640 lines can be resolved if we postulate that both lines are formed in a halo surrounding the

TABLE 4—*Continued*

TEFF=22500. LOG(G)= 8.00 ML2. PURE He				TEFF=25000. LOG(G)= 8.00 ML2. PURE He			
M	TEMP	NE	NTOT	M	TEMP	NE	NTOT
7.768E-07	1.406E+04	1.612E+13	4.002E+13	7.768E-07	1.480E+04	1.725E+13	3.803E+13
1.104E-06	1.454E+04	2.311E+13	5.503E+13	1.104E-06	1.512E+04	2.413E+13	5.289E+13
1.546E-06	1.465E+04	3.131E+13	7.646E+13	1.546E-06	1.521E+04	3.304E+13	7.362E+13
2.137E-06	1.477E+04	4.191E+13	1.048E+14	2.137E-06	1.533E+04	4.460E+13	1.010E+14
2.920E-06	1.492E+04	5.560E+13	1.417E+14	2.920E-06	1.547E+04	5.958E+13	1.367E+14
3.934E-06	1.508E+04	7.293E+13	1.890E+14	3.934E-06	1.563E+04	7.862E+13	1.823E+14
5.258E-06	1.523E+04	9.492E+13	2.500E+14	5.258E-06	1.581E+04	1.030E+14	2.409E+14
6.990E-06	1.539E+04	1.228E+14	3.290E+14	6.990E-06	1.599E+04	1.343E+14	3.166E+14
9.274E-06	1.554E+04	1.580E+14	4.322E+14	9.274E-06	1.619E+04	1.749E+14	4.150E+14
1.222E-05	1.568E+04	2.009E+14	5.647E+14	1.222E-05	1.638E+04	2.261E+14	5.403E+14
1.608E-05	1.579E+04	2.534E+14	7.377E+14	1.608E-05	1.658E+04	2.916E+14	7.028E+14
2.122E-05	1.588E+04	3.179E+14	9.678E+14	2.122E-05	1.677E+04	3.767E+14	9.167E+14
2.813E-05	1.597E+04	4.000E+14	1.276E+15	2.813E-05	1.695E+04	4.884E+14	1.202E+15
3.726E-05	1.607E+04	5.063E+14	1.679E+15	3.726E-05	1.713E+04	6.322E+14	1.575E+15
4.967E-05	1.621E+04	6.488E+14	2.219E+15	4.967E-05	1.730E+04	8.214E+14	2.079E+15
6.674E-05	1.632E+04	8.254E+14	2.962E+15	6.674E-05	1.744E+04	1.066E+15	2.772E+15
9.046E-05	1.640E+04	1.042E+15	3.996E+15	9.046E-05	1.747E+04	1.364E+15	3.750E+15
1.236E-04	1.644E+04	1.303E+15	5.446E+15	1.236E-04	1.749E+04	1.741E+15	5.121E+15
1.704E-04	1.644E+04	1.601E+15	7.510E+15	1.704E-04	1.749E+04	2.212E+15	7.057E+15
2.373E-04	1.644E+04	1.975E+15	1.045E+16	2.373E-04	1.751E+04	2.817E+15	9.817E+15
3.339E-04	1.645E+04	2.442E+15	1.470E+16	3.339E-04	1.754E+04	3.593E+15	1.379E+16
4.742E-04	1.647E+04	3.026E+15	2.085E+16	4.742E-04	1.759E+04	4.608E+15	1.953E+16
6.793E-04	1.650E+04	3.775E+15	2.982E+16	6.793E-04	1.766E+04	5.951E+15	2.786E+16
9.805E-04	1.654E+04	4.746E+15	4.293E+16	9.805E-04	1.776E+04	7.740E+15	3.999E+16
1.424E-03	1.660E+04	6.020E+15	6.211E+16	1.424E-03	1.788E+04	1.015E+16	5.769E+16
2.076E-03	1.669E+04	7.702E+15	9.014E+16	2.076E-03	1.804E+04	1.350E+16	8.336E+16
3.033E-03	1.679E+04	9.954E+15	1.309E+17	3.033E-03	1.828E+04	1.835E+16	1.202E+17
4.427E-03	1.694E+04	1.308E+16	1.893E+17	4.427E-03	1.862E+04	2.586E+16	1.722E+17
6.429E-03	1.715E+04	1.764E+16	2.715E+17	6.429E-03	1.916E+04	3.864E+16	2.430E+17
9.252E-03	1.746E+04	2.473E+16	3.837E+17	9.252E-03	2.007E+04	6.303E+16	3.338E+17
1.312E-02	1.796E+04	3.712E+16	5.289E+17	1.312E-02	2.169E+04	1.140E+17	4.380E+17
1.822E-02	1.877E+04	6.114E+16	7.031E+17	1.822E-02	2.422E+04	2.014E+17	5.448E+17
2.472E-02	2.208E+04	1.872E+17	8.109E+17	2.472E-02	2.684E+04	2.911E+17	6.667E+17
3.232E-02	2.421E+04	3.130E+17	9.667E+17	3.232E-02	2.917E+04	3.735E+17	8.022E+17
4.057E-02	2.599E+04	4.320E+17	1.131E+18	4.057E-02	3.105E+04	4.508E+17	9.461E+17
5.057E-02	2.771E+04	5.569E+17	1.321E+18	5.057E-02	3.290E+04	5.380E+17	1.113E+18
5.855E-02	2.906E+04	6.477E+17	1.459E+18	5.855E-02	3.418E+04	6.032E+17	1.240E+18
6.906E-02	3.087E+04	7.491E+17	1.620E+18	6.906E-02	3.562E+04	6.856E+17	1.403E+18
7.847E-02	3.253E+04	8.282E+17	1.747E+18	7.847E-02	3.686E+04	7.556E+17	1.541E+18
8.674E-02	3.395E+04	8.890E+17	1.850E+18	8.674E-02	3.780E+04	8.164E+17	1.661E+18
9.936E-02	3.557E+04	9.805E+17	2.023E+18	9.936E-02	3.924E+04	9.028E+17	1.833E+18
1.178E-01	3.775E+04	1.105E+18	2.259E+18	1.178E-01	4.115E+04	1.024E+18	2.072E+18
1.464E-01	4.027E+04	1.294E+18	2.632E+18	1.464E-01	4.402E+04	1.197E+18	2.407E+18
1.985E-01	4.488E+04	1.590E+18	3.202E+18	1.985E-01	4.950E+04	1.477E+18	2.902E+18
2.708E-01	4.986E+04	1.992E+18	3.932E+18	2.708E-01	5.350E+04	1.915E+18	3.664E+18
3.557E-01	5.277E+04	2.505E+18	4.880E+18	3.557E-01	5.601E+04	2.441E+18	4.597E+18
4.435E-01	5.508E+04	3.032E+18	5.829E+18	4.435E-01	5.819E+04	2.975E+18	5.517E+18
4.987E-01	5.612E+04	3.363E+18	6.432E+18	4.987E-01	5.919E+04	3.307E+18	6.098E+18

star. This may well be the first occurrence in the DB white dwarfs of a phenomenon already recognized in many hydrogen-rich DA stars.

In the DB white dwarfs the temperature and densities throughout the photosphere are such that most of the helium is in the neutral state and particularly the resonance lines of He I at 522, 537 and 584 Å are *very* strong and their red wings have an important effect on the emergent flux even as far as up to the peak of the energy distribution, and beyond. Attention could profitably be paid to the accurate modeling of these strong lines.

Finally, we established that the uncertainties on the modeling of helium model atmospheres characteristic of the DB white dwarfs are relatively small. We make our grid of DB models available upon request.

It is a pleasure to thank Detlev Koester and Francois Wesemael for many helpful comments concerning this project and

TABLE 4—*Continued*

TEFF=27500. LOG(G)= 8.00 ML2. PURE He				TEFF=30000. LOG(G)= 8.00 ML2. PURE He			
M	TEMP	NE	NTOT	M	TEMP	NE	NTOT
7.768E-07	1.595E+04	1.714E+13	3.528E+13	7.768E-07	1.725E+04	1.622E+13	3.262E+13
1.104E-06	1.610E+04	2.405E+13	4.967E+13	1.104E-06	1.731E+04	2.295E+13	4.620E+13
1.546E-06	1.617E+04	3.332E+13	6.928E+13	1.546E-06	1.734E+04	3.202E+13	6.461E+13
2.137E-06	1.624E+04	4.543E+13	9.530E+13	2.137E-06	1.738E+04	4.400E+13	8.907E+13
2.920E-06	1.635E+04	6.117E+13	1.294E+14	2.920E-06	1.743E+04	5.971E+13	1.213E+14
3.934E-06	1.648E+04	8.118E+13	1.729E+14	3.934E-06	1.751E+04	7.978E+13	1.627E+14
5.258E-06	1.664E+04	1.068E+14	2.289E+14	5.258E-06	1.762E+04	1.055E+14	2.162E+14
6.990E-06	1.682E+04	1.398E+14	3.010E+14	6.990E-06	1.775E+04	1.387E+14	2.852E+14
9.274E-06	1.702E+04	1.827E+14	3.946E+14	9.274E-06	1.792E+04	1.818E+14	3.749E+14
1.222E-05	1.724E+04	2.371E+14	5.135E+14	1.222E-05	1.811E+04	2.364E+14	4.888E+14
1.608E-05	1.746E+04	3.074E+14	6.670E+14	1.608E-05	1.832E+04	3.068E+14	6.358E+14
2.122E-05	1.770E+04	3.994E+14	8.686E+14	2.122E-05	1.856E+04	3.990E+14	8.283E+14
2.813E-05	1.793E+04	5.211E+14	1.136E+15	2.813E-05	1.881E+04	5.210E+14	1.083E+15
3.726E-05	1.815E+04	6.787E+14	1.487E+15	3.726E-05	1.906E+04	6.796E+14	1.416E+15
4.967E-05	1.835E+04	8.885E+14	1.960E+15	4.967E-05	1.930E+04	8.921E+14	1.863E+15
6.674E-05	1.850E+04	1.168E+15	2.612E+15	6.674E-05	1.952E+04	1.180E+15	2.477E+15
9.046E-05	1.859E+04	1.540E+15	3.525E+15	9.046E-05	1.968E+04	1.574E+15	3.328E+15
1.236E-04	1.862E+04	2.029E+15	4.808E+15	1.236E-04	1.978E+04	2.112E+15	4.526E+15
1.704E-04	1.865E+04	2.674E+15	6.618E+15	1.704E-04	1.984E+04	2.848E+15	6.221E+15
2.373E-04	1.868E+04	3.529E+15	9.200E+15	2.373E-04	1.990E+04	3.860E+15	8.639E+15
3.339E-04	1.875E+04	4.674E+15	1.290E+16	3.339E-04	1.999E+04	5.257E+15	1.210E+16
4.742E-04	1.884E+04	6.226E+15	1.823E+16	4.742E-04	2.012E+04	7.199E+15	1.706E+16
6.793E-04	1.897E+04	8.341E+15	2.593E+16	6.793E-04	2.030E+04	9.913E+15	2.423E+16
9.805E-04	1.913E+04	1.125E+16	3.712E+16	9.805E-04	2.054E+04	1.375E+16	3.457E+16
1.424E-03	1.936E+04	1.538E+16	5.328E+16	1.424E-03	2.087E+04	1.927E+16	4.940E+16
2.076E-03	1.968E+04	2.146E+16	7.641E+16	2.076E-03	2.136E+04	2.743E+16	7.038E+16
3.033E-03	2.016E+04	3.090E+16	1.089E+17	3.033E-03	2.208E+04	3.971E+16	9.947E+16
4.427E-03	2.092E+04	4.639E+16	1.533E+17	4.427E-03	2.312E+04	5.809E+16	1.386E+17
6.429E-03	2.210E+04	7.250E+16	2.107E+17	6.429E-03	2.454E+04	8.422E+16	1.897E+17
9.252E-03	2.382E+04	1.127E+17	2.812E+17	9.252E-03	2.625E+04	1.184E+17	2.552E+17
1.312E-02	2.587E+04	1.629E+17	3.671E+17	1.312E-02	2.809E+04	1.612E+17	3.381E+17
1.822E-02	2.800E+04	2.204E+17	4.711E+17	1.822E-02	2.995E+04	2.130E+17	4.403E+17
2.472E-02	2.982E+04	2.866E+17	6.001E+17	2.472E-02	3.182E+04	2.743E+17	5.623E+17
3.232E-02	3.197E+04	3.549E+17	7.318E+17	3.232E-02	3.364E+04	3.411E+17	6.954E+17
4.057E-02	3.314E+04	4.315E+17	8.861E+17	4.057E-02	3.529E+04	4.091E+17	8.322E+17
5.057E-02	3.545E+04	5.064E+17	1.032E+18	5.057E-02	3.713E+04	4.862E+17	9.857E+17
5.855E-02	3.610E+04	5.762E+17	1.174E+18	5.855E-02	3.842E+04	5.451E+17	1.103E+18
6.906E-02	3.822E+04	6.451E+17	1.308E+18	6.906E-02	4.010E+04	6.173E+17	1.246E+18
7.847E-02	3.897E+04	7.192E+17	1.458E+18	7.847E-02	4.148E+04	6.799E+17	1.369E+18
8.674E-02	4.031E+04	7.703E+17	1.557E+18	8.674E-02	4.280E+04	7.306E+17	1.467E+18
9.936E-02	4.187E+04	8.521E+17	1.718E+18	9.936E-02	4.455E+04	8.077E+17	1.614E+18
1.178E-01	4.393E+04	9.668E+17	1.940E+18	1.178E-01	4.783E+04	9.069E+17	1.782E+18
1.464E-01	4.825E+04	1.115E+18	2.196E+18	1.464E-01	5.268E+04	1.071E+18	2.010E+18
1.985E-01	5.347E+04	1.424E+18	2.686E+18	1.985E-01	5.651E+04	1.406E+18	2.540E+18
2.708E-01	5.642E+04	1.884E+18	3.474E+18	2.708E-01	6.011E+04	1.865E+18	3.260E+18
3.557E-01	5.937E+04	2.409E+18	4.336E+18	3.557E-01	6.282E+04	2.391E+18	4.096E+18
4.435E-01	6.131E+04	2.947E+18	5.236E+18	4.435E-01	6.521E+04	2.918E+18	4.922E+18
4.987E-01	6.242E+04	3.280E+18	5.782E+18	4.987E-01	6.640E+04	3.237E+18	5.434E+18

for having made available to us their new models. We are grateful to Jim Liebert for his careful reading of the manuscript. We are also sincerely grateful to Franziska Eber and Sylvie Beaulieu for providing us with comparative models from their atmosphere programs, and Thomas Schöning who very kindly provided us with machine-readable tables of He II Stark-broadened line profiles. Support from the NSF (grant AST 87-20530), NASA (grant NAG 5-348) and the Danish Research Academy 880070 is acknowledged.

Note added in manuscript.—The temperature of GD 358 suggested here settles a long-standing controversy which was formalized in the form of a wager at the 5th European Workshop on White Dwarfs held in Kiel, 1984. The authors of this paper and the other participants in the 7th European Workshop on White Dwarfs held in Toulouse, 1990, gratefully acknowledge the contributions of Prof. Volker Weidemann (winner) and Jim Liebert (loser) to the convivial atmosphere following the latter workshop.

REFERENCES

Auer, L. H., & Mihalas, D. 1972, ApJS, 24, 193
Barnard, A. J., Cooper, J., & Shamey, L. J. 1969, A&A, 1, 28
Bhatia, S., Shipman, H. L., Thejll, P. A., & Liebert, J. 1989, BAAS, 21, 1194
Bohlin, R. C., & Grillmair, C. J. 1988, ApJS, 68, 487
Böhm, K. H., & Cassinelli, J. 1971, A&A, 12, 21
Böhm, K. H., & Grenfell, T. C. 1973, A&A, 28, 79
D'Antona, F. 1988, in IAU Coll. 114, White Dwarfs, ed. G. Wegner (Berlin: Springer), p. 44
de Loore, C. 1970, ASpSc, 6, 60
Dimitrijevic, M. S., & Sahal-Brechot, S. 1984a, JQSRT, 31, 301
———. 1984b, A&A, 136, 289
Finley, D., Basri, G., & Bowyer, S. 1990, ApJ, 359, 483
Fontaine, G., Tassoul, M., & Wesemael, F. 1984, in Proceedings of the 25th Liege International Astrophysical Colloquium: Theoretical Problems in Stellar Stability and Oscillations (Liege: Universite de Liege), p. 328
Fontaine, G., Villeneuve, B., & Wilson, J. 1981, ApJ, 243, 550
Grauer, A. D., Bond, H. E., Green, R. F., & Liebert, J. 1988, AJ, 95, 879
Grauer, A. D., Wegner, G., Green, R. F., & Liebert, J. 1989, AJ, 98, 2221
Greenstein, J. L. 1984 ApJ, 276, 602
Greenstein, J. L., & Liebert, J. 1990, ApJ, in press.
Greenstein, J. L. Oke, J. B., Richstone, D., Van Altena, W. F., & Steppe, H. 1977, ApJ, 218, L21
Griem, H. R. 1974, Spectral Line Broadening by Plasmas (New York: Academic Press)
Höhne, F. E., & Zimmermann, R. 1982, JPB, 15, 2551
Koester, D. 1980, A&AS 39, 401
———. 1990, private communication
Koester, D., Vauclair, G., Dolez, N., Oke, J. B., Greenstein, J. L., & Weidemann, V. 1985, A&A, 149, 423
Koester, D., Weidemann, V., & Vauclair, G. 1983, A&A, 123, L11
Kurucz, R. L. 1970, SAOSpRp, 309
Liebert, J., Wesemael, F., Hansen, C. J., Fontaine, G., Shipman, H. L., Sion, E. M., Winget, D. E., & Green, R. F. 1986, ApJ, 309, 241 (L86)
MacDonald, J., & Vennes, S. 1990, ApJ, in press
Oke, J. B. 1974, ApJS, 27, 21
Oke, J. B., Weidemann, V., & Koester, D. 1984, ApJ, 281, 276
Pelletier, C., Fontaine, G., Wesemael, F., Michaud, G., & Wegner, G. 1986, ApJ, 307, 242
Reid, N., Wegner, G., Wickramansinghe, D. T., & Bessell, M. S. 1988, AJ, 96, 275
Schöning, T., & Butler, K. 1989a, A&AS, 79, 153
———. 1989b, A&AS, 78, 51
Seaton, M. J. 1979, MNRAS, 187, 73P
Shipman, H. L. 1979, ApJ, 228, 240
Sion, E. M., Liebert, J., Vauclair, G., & Wegner, G. 1988, in IAU Coll. 114, White Dwarfs, ed. G. Wegner (Berlin: Springer), p. 354
Wegner, G., & Nelan, E. P. 1987, ApJ, 319, 916
Wesemael, F. 1981, ApJS, 45, 177 (W81)
———. 1990, private communication
Wickramasinghe, D. T. 1983, MNRAS, 203, 903
Wickramasinghe, D. T., & Reid, N. 1983, MNRAS, 203, 887
Wickramasinghe, D. T., & Whelan, J. A. J. 1977, MNRAS, 178, 11P
Winget, D. E., Nather, R. E., & Hill, J. A. 1987, ApJ, 316, 305
Winget, D. E., Robinson, E. L., Nather, R. E., & Balachandran, S. 1984, ApJ, 279 L15
Winget, D. E., Robinson, E. L., Nather, R. E., & Fontaine, G. 1982, ApJ, 262, L11
Winget, D. E., Van Horn, H. M., Tassoul, M., Hansen, C. J., & Fontaine, G. 1983, ApJ, 268, L33